J. Chin. Inst. Chem. Engrs., Vol. 36, No. 5, 497-509, 2005

Measurements of the Particle Velocity and Flow Pattern of Particles in Magnetically Fluidized Beds

Yung-Chung Lin [1] and Lii-Ping Leu[2]
Department of Chemical Engineering, National Taiwan University
Taipei 106, Taiwan

Abstract—The particle velocity and flow pattern of particles in fluidized beds of iron particles (230 μm) were investigated under the influence of an external uniform axial magnetic field. A uniform magnetic field was generated by passing a direct current through five solenoids. A sensitive optical measuring system, based on the detection of light reflected by particles, was used to measure the particle velocity in the dense phase.

The particle velocity was measured as a function of the superficial fluidizing air velocity, magnetic field intensity and position in the bed. The experimental results revealed that the particle velocity was zero in a magnetically stabilized fluidized bed (MSFB). The particle velocity in a magnetized bubbling fluidized bed (MBFB) decreased as the magnetic field intensity and radial distance from the axis of bed column increased, and as the superficial gas velocity, and axial distance from the distributor decreased. The magnitude and direction of the particle velocity were calculated by using the equation: $V_p = L_{ef} /(\tau_r^2 + \tau_z^2)^{1/2}$ and $\theta = \tan^{-1}(\tau_z / \tau_r)$. The following general correlation was developed to predict the axial transit time (τ_z): $1/\tau_z = 1/\tau_{zc} - (1/\tau_{zc} - 1/\tau_{zw})\ (r/R)^B$, where τ_{zc} and τ_{zw} represent the axial transit time at the bed center and at the bed wall, respectively, and B is a parameter. All were functions of the air velocity, the distance from the distributor and the magnetic field intensity, and all had similar forms as follows : $A1(z/h_s)^{A2}(U_s/U_{mf})^{A3}\{\exp[A4(z/h_s)+A5(U_s/U_{mf})]\}H^{A6}$. Results obtained in time-averaged particle velocity experiments were close to those obtained through simulation.

Key Words : Fluidized beds, Magnetically fluidized beds, Particle velocity, Optical fiber probe

INTRODUCTION

A fluidized bed of magnetizable particles under the influence of an external magnetic field is called a magnetofluidized bed (MFB). An expanded MFB without bubbles is called a magnetically stabilized fluidized bed (MSFB). An MSFB is a fluid-particle contactor that shares a number of advantages with packed beds and fluidized beds. Similar to fluidized beds, the solids in an MFB resemble a liquid and are easily transported between vessels. The loading of particles is also easier as the particles move in and out of the bed continuously. Because the magnetic forces in an MSFB suppress the formation of bubbles, its contacting efficiencies are close to those of a fixed bed without gas bubbles or solid back mixing. Local temperatures and particle distributions in an MSFB are much more uniform than those in fixed beds. The gas phase flows through the MSFB in nearly plug flow and has a narrow residence time distribution similar to that of fixed beds. MSFBs are used extensively in affinity chromatography, aerosol filtration, particle separation, biological separation, gas separation, ammonia synthesis, and ethanol fermentation. A review of research on these topics can be found elsewhere (Liu *et al.*, 1991). An MFB with bubbles is called a magnetically bubbling fluidized bed (MBFB). By regulating the magnetic field intensity and superficial gas velocity in an MBFB, one can obtain a desired radial voidage profile and bubble size (Lin and Leu, 2001; Jovanovic *et al.*, 1989; Jovanovic and Jovanovic, 1993). Examination of the flow properties of particles is essential to the design and application of MFBs.

The available techniques for local particle velocity measurement can essentially be classified into seven categories: (1) drag force methods (Heertjes *et al.*, 1970; Botterill and Bessant, 1976; Raso *et al.*, 1983), (2) heat transfer methods (Marsheck and Gomezplata, 1965), (3) electrostatic probe methods (Klinzing *et al.*,1987), (4) laser Doppler velocimetry methods (Levy and Lockwood, 1983; Tsuji *et al.*, 1984; Yianneskis, 1987; Yang *et al.*, 1992), (5) fluorescent particle methods (Hamdullahpur *et al.*, 1987; Morooka *et al.*, 1989), (6) tracer methods (Rao and Venkateswarlu, 1973; Merry and Davidson, 1973;

[1] 林永忠
[2] 呂理平, To whom all correspondence should be addressed

van Velzen *et al.*, 1974; Stein *et al.*, 2000) and (7) statistical correlation methods (Oki and Walawender, 1977; Patrose and Caram, 1982; Nieuwland *et al.*, 1996; Zhang and Zhu, 2000). A correlation technique in conjunction with a fiber optical system is the most widely-used method. Many researches have studied on the local particle velocity in circulating fluidized beds (CFBs) by using reflective optical probe systems (Nieuwland *et al.*, 1996; Horio *et al.*, 1988; Hartge *et al.*,1988; Herbert *et al.*, 1994; Tung *et al.*, 1988; Zhang *et al.*, 1991). Only a few works have studied local particle velocity measurement in dense fluidized beds (Patrose and Caram, 1982; Dencs, 1995). The reason may be the complexity of the dense beds. The local velocity measured in CFBs (dilute phase) is the velocity of clusters (a group of particles), while the local velocity in MFBs or bubbling beds (dense phase) is the velocity of a single particle. For Geldart group A and B powders (Geldart, 1973) in CFBs, the ratio of the maximum cluster diameter to the particle diameter is about 140 and 20, respectively (Xia *et al.*, 1993). The size of a single particle is smaller than that of a cluster. Therefore, determining of the particle velocity in MFBs or bubbling beds is more difficult than in CFBs. The size of the probe must be small enough for it to be able to detect light reflected from individual particles. The smaller the particles are, the more difficult it is to design the probe. Usually, the mean diameter of particles in studies performed using reflective optical probes have been between 500 μm and 1118 μm (Patrose and Caram, 1982; Dencs, 1995). A new optical fiber probe which can be used to determine the velocity of a single particle whose mean diameter is smaller than 500 μm in the dense phase is needed. The purpose of this study was to develop a new optical fiber probe that can be used to measure the velocity of small individual particles (iron particles of Geldart group B powders, d_p= 230 μm, were used here) in MFBs in order to study the particle motion and obtain detailed information about the particle dynamics, which is crucial for the design and application of MFBs.

EXPERIMENTAL FACILITY

The experimental facility is shown schematically in Fig. 1. It consisted of an air supply system, a fluidization column, a specially designed electromagnet, an off-gas cleaning system and a data acquisition system. The fluidization column was constructed from 1 cm thick 100 cm long transparent Plexiglas pipe with a 5 cm i.d. The column was equipped with a perforated distributor with a 4.96 %-open area. Five solenoids with a 22.6 cm inner diameter, 2 cm axial width and 2,663 turns of 19 SWG

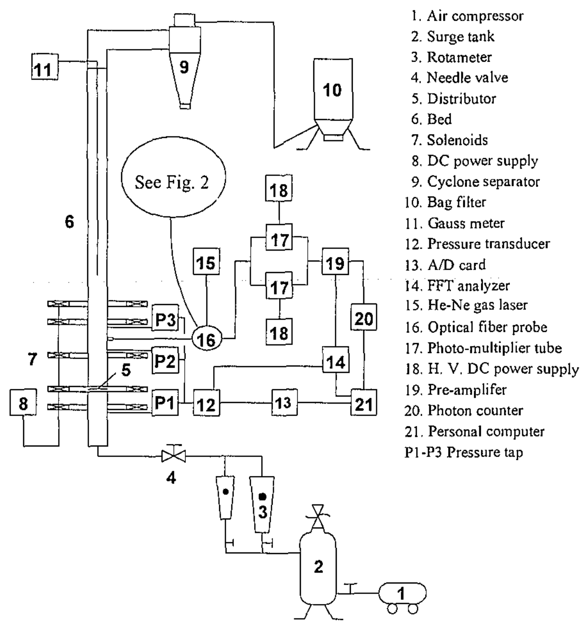

Fig. 1. Experimental setup.

magnet wire were used to generate an axial magnetic field. The distance between the midpoints of the axial widths of the two solenoids is 11.3 cm or 5.8 cm. The magnetic field intensity distribution obtained by using this specially designed electromagnet is shown elsewhere (Lin and Leu, 2001).

An optical fiber probe was installed at different levels above the distributor along the bed, and it could be moved horizontally for measurements at different radial positions. 1706.1 g of iron particles were fed into the fluidization column. The static bed height (h_s) was 18.9 cm. The measured particle velocity was the local, time-averaged value for each radial position. The sampling frequency was set to 2-20 kHz. For a lower particle velocity, a lower sampling frequency could be used. Each velocity value reported here is the average of more than 300 sampled velocities. The signal sequences on two receiving fibers can not be processed with the cross-correlation method (Oki and Walawender, 1977) because of the complexity of the motion of the particles in the MFBs and the small size of the particles. The smaller the size of particles is, the more stochastic the signal sequences are. Therefore, here the voltage values recorded in an analyzer were used to process by means of the transit time method (Patrose and Caram, 1982). The particle velocity was measured at eight radial positions between the bed wall and the center of the bed, because eight points were considered sufficient to construct the particle velocity profile in the bed, which had a 5 cm i.d. When the particle velocity was measured, a magnetic field was applied at a fixed superficial gas velocity to the particles, which were already fluidized; the mode of this operation was the "magnetization

Table 1. The properties of the solid particles.

Solid Particles	Iron
Classification of Geldart particles	Group B
Shape	Spherical
Size range (μm)	212-250
Mean diameter (μm)	230
True density (kg/m^3)	7860
Minimum fluidization velocity, U_{mf} [a] (m/s)	0.135
Terminal velocity, V_t [b] (m/s)	4.276

[a] Measured value without an applied magnetic field.
[b] Calculated value.

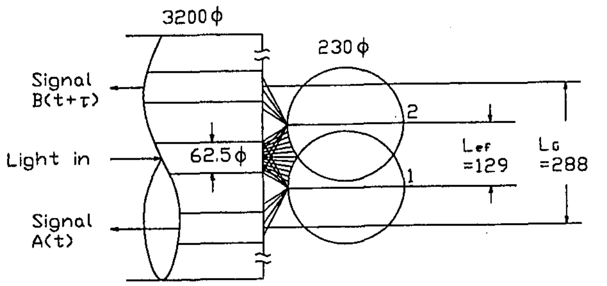

Fig. 2. Optical fiber probe (dimensions are in μm).

LAST" mode, according to the classification of Hristov (1998). The properties of the solid particles used in this study are listed in Table 1.

OPTICAL FIBER PROBE CALIBRATION AND MEASUREMENT TECHNIQUE

An optical fiber probe with a length of 15 cm and a diameter 3.2 mm was specially designed for taking measurements of the particle velocity in the dense beds studied here. The optical fiber probe consisted of three 62.5 μm core diameter glass optical fibers (Fig. 2). One central optical fiber was used to illuminate the measuring site. The light source was a 5 mW He-Ne laser. Light was reflected back by a particle at the tip of an illuminated probe into two other optical fibers located above and below the central optical fiber. Figure 3 shows the time difference of two signal sequences. The time delay between the two signals was obtained by calculating the time difference. If the trajectory of a particle was parallel to the connecting line of the two receiving fibers, the particle velocity was calculated by using the following equation:

$$V_p = L_{ef} / \tau, \quad (1)$$

where V_p = the particle velocity (m/s), L_{ef} = the effective distance between two light-detecting fibers (m), and τ = the transit time (s).

The effective distance between the receiving fibers is slightly different from the geometrical distance (Patrose and Caram, 1982). In order to obtain

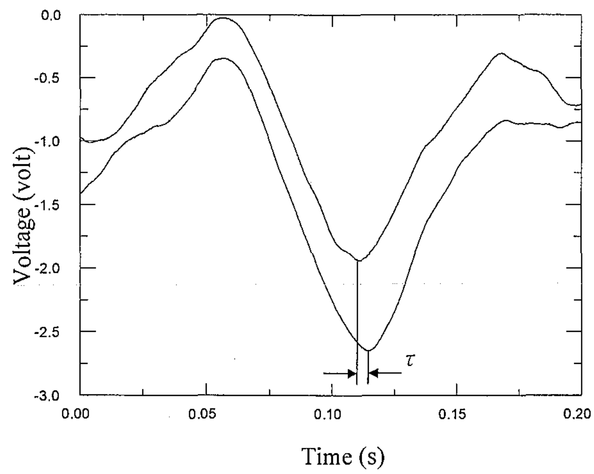

Fig. 3. Time difference of two signal sequences.

the effective distance for the probe used in this work, the calibration procedure was carried out with a probe placed inside a bed of iron particles with a size range of 212-250 μm in a cylindrical container. The container was rotated by using a DC motor (Oki *et al.*, 1975). The speed of the particles could be varied and controlled by adjusting the angular speed of the motor. The angular velocity ω was calculated by using the following equation:

$$\omega = 2\pi / T, \quad (2)$$

where T = the period of a rotation (s). The particle velocity in the cylindrical container (V_p) was calculated by using the following equation:

$$V_p = R_{rtt}\omega, \quad (3)$$

where R_{rtt} = the distance between the tip of the probe and the center of the rotating bed. The particle velocity and the transit time were used to compute the effective fiber-to-fiber separation distance L_{ef}.

Table 2 includes a representative set of calibration data. The average effective distance (the mean value of eight effective distances) was found to be 129 μm. An effective distance of 129 μm was to be small enough for the detection of reflected light from individual particles (d_p>64.5 μm), whereas the actual geometric center-to-center distance between the two receiving fibers was measured under the microscope and found to be 288 μm. If such a probe consists of only two receiving fibers (no central fiber as shown in Fig. 2) and the two receiving fibers are also used to illuminate the measuring site (*i.e.*, light in and out with the same fiber), then the effective distance between the two receiving fibers will be the same as the geometric center-to-center distance between the two receiving fibers. However, the strength of the signal of a two-fiber probe of this

Table 2. Computation of effective distance L_{ef}.

Particle Velocity V_p (m/s) = $R_{rtt}\,\omega$	Transit Time τ (μs)	Effective Distance L_{ef} (μm) = $V_p\tau$	Mean Effective Distance L_{ef} (μm)
0.0310	4160	129	
0.0868	1406	122	
0.1390	957	133	
0.1943	664	129	129
0.2486	527	131	
0.3293	410	135	
0.4725	273	129	
0.5907	215	127	

Note: R_{rtt} = 8.8 cm in this work.

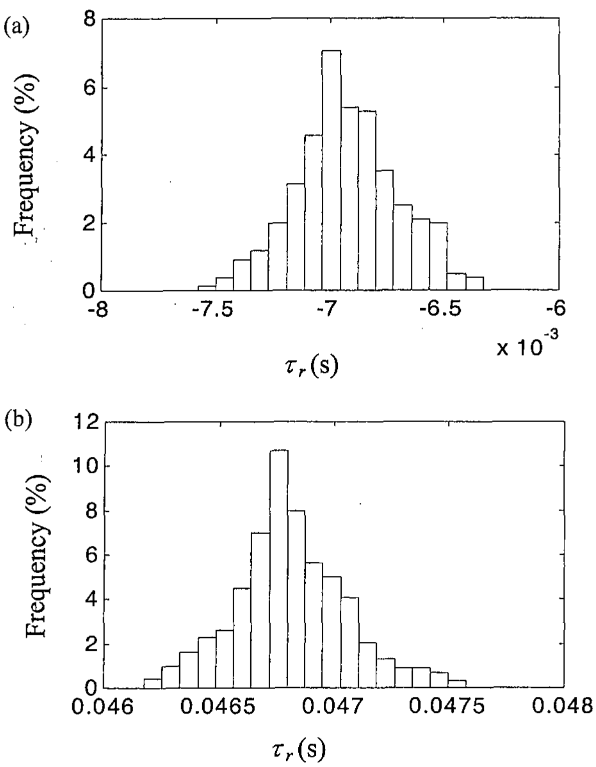

Fig. 4. Radial transit time profile (H = 0 A/m; U_s/U_{mf} = 1.42; r/R = 0.8; z/h_s = 0.878; sampling frequency = 5 kHz; (a) particles move to the bed center; (b) particles move to the bed wall).

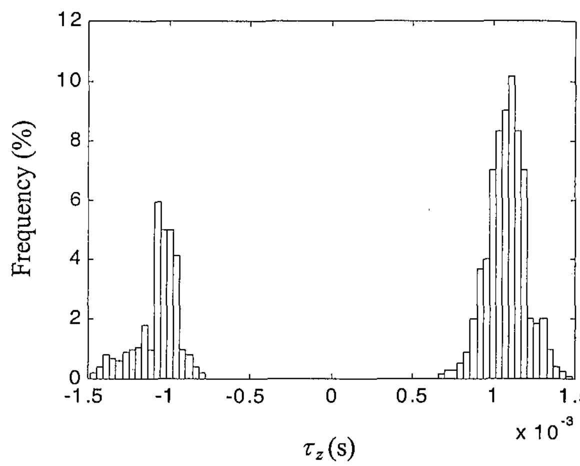

Fig. 5. Axial transit time profile (H = 0 A/m, U_s/U_{mf} = 1.42; r/R = 0; z/h_s = 0.878; sampling frequency = 10 kHz).

kind is too small to measure the velocity of small individual particles properly. Therefore, a three-fiber probe as shown in Fig. 2 was used here to measure the velocity of small individual particles. In this situation, the effective distance was different from the actual center-to-center distance.

If the trajectory of a moving particle is not parallel to the connecting line of the two receiving fibers, then the method for calculating the particle velocity is similar to that used by Patrose and Caram (1982) with the following equations:

$$V_p = L_{ef}/(\tau_r^2 + \tau_z^2)^{1/2}, \tag{4}$$

and

$$\theta = \tan^{-1}(\tau_z/\tau_r), \tag{5}$$

where τ_r, τ_z = the transit time in the radial or axial direction, and θ = the flow orientation with respect to the horizontal. Figures 4 and 5 show the τ_r and τ_z frequency profiles. When τ_r was measured, the connecting line of the two receiving fibers was perpendicular to the axis of the bed column, and the receiving fiber A (light out (t) in Fig. 2) was on the left side of the receiving fiber B (light out $(t+\tau)$ in Fig. 2). At this instant, the distance between the receiving fiber A and the bed center was smaller than that between the receiving fiber B and the bed center. When τ_z was measured, the connecting line of the two receiving fibers was parallel to the axis of the bed column, and the receiving fiber A (light out (t) in Fig. 2) was below the receiving fiber B (light out $(t+\tau)$ in Fig. 2). Therefore, the positive τ_r value represented the particles moving to the bed wall, and the negative τ_r value represented the particles moving to the bed center; furthermore, the positive τ_z value represented the particles moving to the top of the bed, and the negative τ_z value represented the particles moving to the bottom of the bed. The range of particle velocity, which this probe could measure, was 0.001-2.2 m/s, and the error range was 4-6 %. The faster the particle

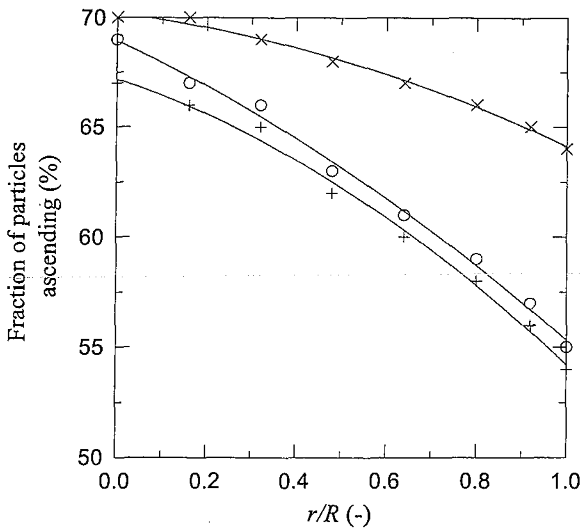

Fig. 6. Radial profiles of fractions of particles traveling upwards at different superficial gas velocities (H = 0 A/m, U_s/U_{mf} = 1.28(+), 1.42(○), 2.22 (×); z/h_s = 0.878).

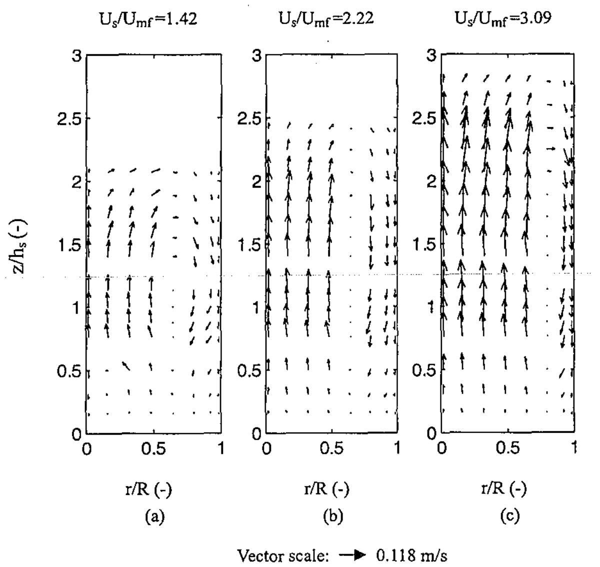

Fig. 7. Particle velocity profiles at various gas velocities without an applied magnetic field (h_s = 0.189 m, H = 0 A/m, (a) U_s/U_{mf}=1.42; (b) U_s/U_{mf}= 2.22; (c) U_s/U_{mf} = 3.09).

velocity was, the larger was the error.

Figure 6 shows the radial profiles of fraction of particles traveling upwards for superficial gas velocities: U_s/U_{mf}=1.28, 1.42, and 2.22 at z/h_s= 0.878 without applying a magnetic field. The fractions of the particles ascending at U_s/U_{mf}=1.28, 1.42, and 2.22 at the bed center were 67, 69, and 70 %, respectively; and at the bed wall were 54, 55, and 64 %, respectively. The method used to calculate the fractions of the particles ascending, the fractions of the particles descending and the particle velocity in the fluidized beds can be found elsewhere (Lin, 2001) and will not discuss here.

RESULTS AND DISCUSSION

Flow pattern of particles

From Fig. 7(a) for U_s/U_{mf}= 1.42 without an applied magnetic field, it can be seen that the particles ascended in the bed central region, and descended near the bed wall but both ascended and descended in the near distributor region. The particles circulated as a vortex ring with up flow at the bed axis and down flow at the wall. A second vortex ring formed below the former vortex ring with down flow at the centerline of the bed. This flow pattern is consistent with the result of Stein *et al.* (2000), Werther and Molerus (1973), and Kunii and Levenspiel (1991). They reported that in a deeper fluidized bed (aspect ratio >1) of Geldart group B solids, there are two vortex rings with different flow directions. For the upper vortex ring shown in Fig. 7(a), the demarcation point [$(r/R)_{de}$] between up flow and down flow was 0.64. This result is similar to that obtained by Stein *et al.* (2000); there was an overlapping region between the upward and downward parts of the velocity profiles, *i.e.*, where particles moved both upward and downward. This flow pattern was related to the bubble motion. Particles were moved upwards by rising bubbles and were carried up in their wakes. Because of continuity, the particles moved downwards in regions with less bubble activity. For a uniform gas flow, $U_s > U_{mf}$, a highly expanded gas-solid dispersion formed directly above the distributor. This was unstable, and a few millimeters above the plate the dispersion divided into many little bubbles plus an emulsion phase. Upon rising upward, these bubbles grow very rapidly due to coalescence (Kunii and Levenspiel, 1991). The appearance and coalescence of little bubbles occurred randomly, so medium-sized bubbles could appear at any position in the bed, and large bubbles could appear at any position near the bed surface. Therefore, the break of bubbles did not always occur in the bed central region. When the bubbles broke between the bed center and the bed wall, particles ascended between the bed center and the bed wall, and descended at both the bed center and the bed wall, creating the particle flow pattern shown in Fig. 8(a). When bubbles broke near the bed wall, particles ascended near the bed wall and descended in the bed central region, creating the particle flow pattern shown in Fig. 8(b).

In the slugging regime (Figs. 7(b) and 7(c)) for U_s/U_{mf}= 2.22 and 3.09 without an applied magnetic field, the particles always ascended in the bed central region, and descended near the bed wall; *i.e.*, only one vortex ring formed. The $(r/R)_{de}$ value was still 0.64 at a low fluidizing velocity (U_s/U_{mf} = 2.22), but the $(r/R)_{de}$ value became larger (= 0.8) at a

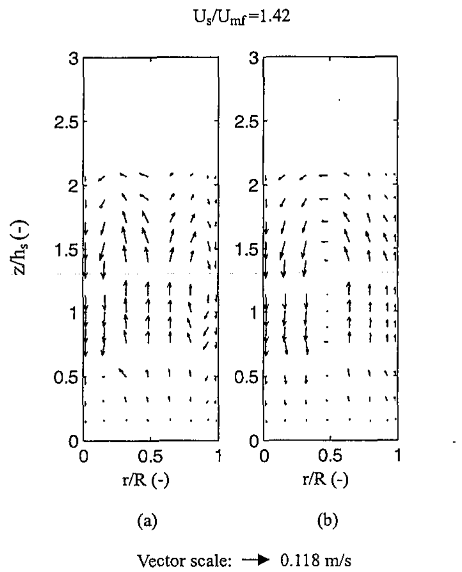

Fig. 8. Particle velocity profiles at various gas velocities without an applied magnetic field (h_s = 0.189 m, H = 0 A/m, (a) bubbles ascend between the bed center and bed wall; (b) bubbles ascend at the bed wall).

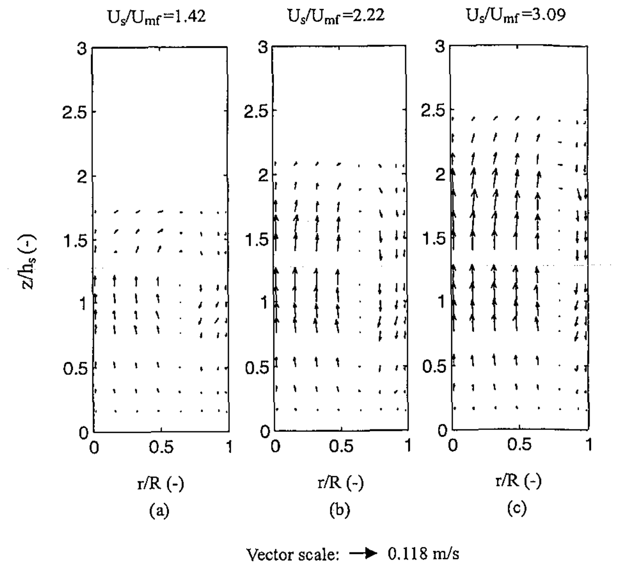

Fig. 9. Particle velocity profiles at various gas velocities with an applied magnetic field (h_s = 0.189 m, H = 858 A/m, (a) U_s/U_{mf}=1.42; (b) U_s/U_{mf}= 2.22; (c) U_s/U_{mf}= 3.09).

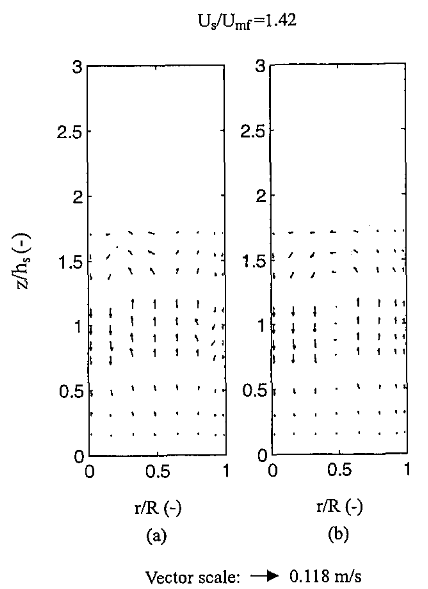

Fig. 10. Particle velocity profiles at various gas velocities with an applied magnetic field. (h_s = 0.189 m, H = 858 A/m, (a) bubbles ascend between the bed center and bed wall; (b) bubbles ascend at the bed wall.)

higher fluidizing velocity (U_s/U_{mf} = 3.09) because the size of bubbles in the slugging regime was larger than that in the bubbling regime. In addition, the bubbles broke the surface preferentially at the bed center. Kunii and Levenspiel (1991) reported a similar result, where at a higher gas flow rate, the solid circulation in the upper vortex ring becomes more vigorous and dominates the overall movement of the emulsion.

At H = 858 A/m and U_s/U_{mf} =1.42 (Fig. 9(a)), the particles ascended in the bed central region and descended near the bed wall. This means that the particles in the deeper fluidized bed under the effect of the magnetic field could not form a second vortex ring. However, when the bubbles broke between the bed center and the bed wall, particles ascended between the bed center and the bed wall, and descended at both the bed center and the bed wall, creating the particle flow pattern shown in Fig. 10(a). When the bubbles broke near the bed wall, particles ascended near the bed wall and descended in the bed central region, creating the particle flow pattern shown in Fig. 10(b).

At H = 858 A/m and U_s/U_{mf} = 2.22 and 3.09 (Figs. 9(b) and 9(c)) in the slugging regime, the size of the bubbles and the height of the bed were smaller than those in the slugging regime without a magnetic field (Figs. 7(b) and 7(c)) because the magnetic field decreased the size of the bubbles and the kinetic energy of the particles, creating similar particle flow patterns.

At a higher magnetic field strength (H = 1716 A/m) and at U_s/U_{mf} = 1.42 (Fig. 11(a)), particles did not move but rather stayed stationary in the bed; this was the MSFB. At U_s/U_{mf} = 2.22 (Fig. 11(b)), the slugging bed changed into a bubbling bed, and the flow pattern of particles was still similar to that at a lower magnetic field strength (Fig. 9(b)). However, the height of the bed was reduced because the magnetic force decreased the bubble size and the kinetic energy of the particles. In addition, when the bubbles broke between the bed center and bed wall, the particles ascended between the bed center and the bed wall, and descended at both the bed center and bed wall, creating the particle flow pattern shown in Fig. 12(a). When bubbles broke near the bed wall, the particles ascended near the bed wall and descended

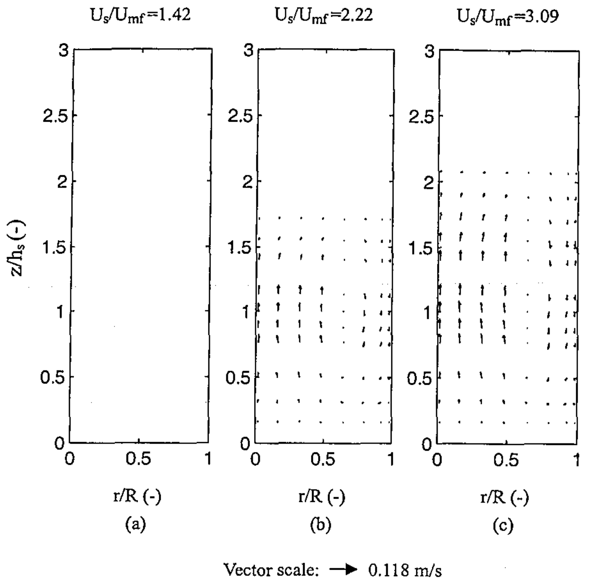

Fig. 11. Particle velocity profiles at various gas velocities with an applied magnetic field (h_s = 0.189 m, H = 1716 A/m, (a) U_s/U_{mf}=1.42; (b) U_s/U_{mf}= 2.22; (c) U_s/U_{mf}= 3.09).

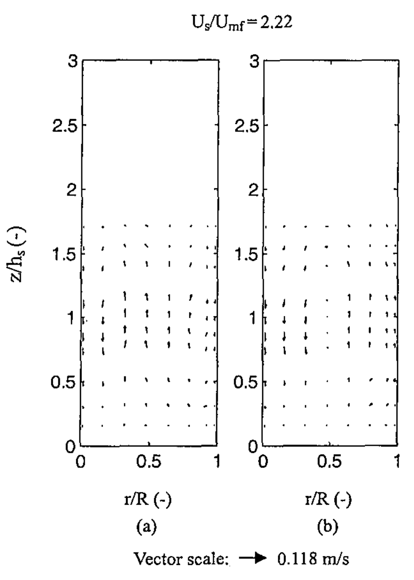

Fig. 12. Particle velocity profiles at various gas velocities with an applied magnetic field (h_s = 0.189 m, H = 1716 A/m, (a) bubbles ascend between the bed center and bed wall; (b) bubbles ascend at the bed wall).

in the bed central region, creating the particle flow pattern shown in Fig. 12(b). At a higher magnetic field strength (H = 1716 A/m) and at U_s/U_{mf} = 3.09 (Fig. 11(c)), the flow pattern of particles was still the same as that without an applied magnetic field (Fig. 7(c)) and at a lower magnetic field strength (Fig. 9(c)). However, the $(r/R)_{de}$ value decreased from 0.8 to 0.64.

Particle velocity profiles

Particle velocity profiles at various radial distances from the axis of the bed column, various distances from the distributor, at various superficial gas velocities, and with and without an applied magnetic field are also shown in Figs. 7-12.

As shown in Figs. 7(a)-7(c), without an applied magnetic field, and at U_s/U_{mf} = 1.42, 2.22, and 3.09, the ascending particle velocity decreased gradually with increasing the radial distance from the axis of the bed column for the case of the fixed distance from the distributor. At the same radial distance from the axis of the bed column, the particle velocity at short distance from the distributor was lower than that at a greater distance from the distributor.

As shown in Figs. 9(a)-9(c), with an applied magnetic field (H = 858 A/m), and at U_s/U_{mf} = 1.42, 2.22, and 3.09, at the same position in the bed, the ascending article velocity at H = 858 A/m was lower than that without a magnetic field (Figs. 7(a)-7(c)), because the magnetic field suppressed bubble formation. Jovanovic and Jovanovic (1993) reported that the bubble size in a G-S fluidized system can be predicted by a parameter – magnetic field deficiency $(H_{ms} - H)$:

$$d_b = 0.005 + 0.0000135\,(H_{ms} - H) \text{ (in SI units)}, \quad (6)$$

where H_{ms} = the minimum stabilization field (the value where the bubble diameter vs. magnetic field intensity curve intersects the abscissa, here denoted as H_{ms}).

From Eq. (6), it can be seen that the larger the magnetic field intensity was, the smaller was the bubble size and the ascending particles in the bubble wake. Therefore, the magnetic field decreased the bubble size and particle velocity at the same time.

In addition, iron particles in the MFB aligned themselves in vertical chains coinciding with the direction of the field. These chains acted as single large particles and became much more resistant to flow than the individual particles. Because the mass of a chain was larger than that of a particle, the chain cleaved a bubble from its roof.

As shown in Fig. 11(a), with an applied magnetic field (H = 1716 A/m), and at U_s/U_{mf} = 1.42, the particle velocity was zero in an MSFB. As shown in Figs. 11(b) and 11(c), with an applied magnetic field (H = 1716 A/m), and at U_s/U_{mf} = 2.22 and 3.09, the particle velocity was smaller than that at H = 858 A/m, because the bubble size became smaller at a higher magnetic field intensity (Jovanovic *et al.*, 1989; Jovanovic and Jovanovic, 1993).

Effect of the magnetic field intensity on the particle velocity

The effect of the magnetic field intensity on the particle velocity at various superficial gas velocities is shown in Figs. 9-12.

At the same position in the bed, the particle velocity at H = 1716 A/m was lower than that at H = 858 A/m. This meant that the stronger the magnetic field intensity was, the greater was the ability to suppress bubble formation, and the fewer particles moved upwards and were carried up in the bubbles' wake.

As shown in Figs. 7(a), 8(a), 9(a), 10(a), 11(a), and 12(a) at U_s / U_{mf} = 1.42, and without or with an applied magnetic field, when the magnetic field intensity increased gradually, particles were arranged along the magnetic field lines, giving an orderly structure to the bed. Thus, the particle velocity decreased gradually. When the magnetic field intensity increased, the bubbles started to disappear and the particle velocity further decreased to zero; *i.e.*, the particles did not move but they were kept stationary in the MSFB. The distance between particles in an MSFB was larger than that in a fixed bed due to bed expansion in the MSFB, so the friction force between particles in an MSFB was smaller than that in a fixed bed.

The gravity force of dense or light objects in an MSFB was smaller than the friction force between particles in a fixed bed, so when they were put into a fixed bed, they could not be readily immersed in the bed. However, the dense and light objects are readily immersed in an MSFB as in a liquid, and when they are released, light objects float and dense objects sink (Rosensweig, 1979). From solid-settling experiments, Lee (1983) found that there are two types of settling kinetics in MSFBs: (1) Light and small particles will approach and stay at equilibrium positions in the bed as a result of the resistance due to yield stress. (2) Heavy and large particles, which are able to overcome the yield resistance, will continue to settle into the MSFBs at, eventually, a constant terminal velocity. Lee (1991) also found that viscoplastic non-Newtonian viscosity and yield stress exist in MSEB media. Therefore, a buoyancy force is exerted on an object in an MSFB. In addition, in a fluidized bed, friction between particles is greatly reduced because the weight of the particles is supported through the fluid flow. There might be a friction-like force owing to the effects of magnetic forces on the particles when they are not strong enough to prevent any movement at all.

Correlation of transit time

At the same distance from the distributor, the maximum radial particle velocity appeared at the demarcation point; *i.e.*, the radial transit time was small. Due to the appearance of vortexes, the change of the radial particle velocity was very irregular. Therefore, it was very difficult to find an equation fitting the radial transit time. However, the change of the axial particle velocity showed a regular trend except at the inflow boundary, outflow boundary and demarcation point. Thus, the following equation could be used to correlate the experimental data of the positive axial transit time (τ_z):

$$1/\tau_z = 1/\tau_{zc} - (1/\tau_{zc} - 1/\tau_{zw})(r/R)^B \qquad (7)$$

or

$$(L_{ef}/\tau_z)/U_{mf} = (L_{ef}/\tau_{zc})/U_{mf} - [(L_{ef}/\tau_{zc})/U_{mf} - (L_{ef}/\tau_{zw})/U_{mf}](r/R)^B, \qquad (8)$$

where τ_{zc} and τ_{zw} represent the axial transit time at the bed center and bed wall, respectively; these values and B are functions of the air velocity, the distance from the distributor and the magnetic field intensity, respectively.

The standard deviation (*S.D.*) of the fitted values (*fit*) from the N experimental values (*exp*) was defined as follows:

$$S.D. = \sqrt{\frac{\sum[(\frac{fit\text{-}exp}{exp})\times 100\%]^2}{N-1}} \times 100(\%). \qquad (9)$$

The value of $(L_{ef}/\tau_{zc})/U_{mf}$ could be calculated using the following equation:

$$(L_{ef}/\tau_{zc})/U_{mf} = (L_{ef}/\tau_{zco})/U_{mf} - 0.09(z/h_s)^{0.1}(U_s/U_{mf})^{0.6} \times \{\exp[0.46(z/h_s) + 0.03(U_s/U_{mf})]\}(H/1000)^{1.1}, \qquad (10)$$

where $(L_{ef}/\tau_{zco})/U_{mf} = 0.830(z/h_s)^{0.4}(U_s/U_{mf})^{1.1} \times\exp[-0.16(U_s/U_{mf})]$ is the $(L_{ef}/\tau_z)/U_{mf}$ value at the bed center without an applied magnetic field. A comparison of $(L_{ef}/\tau_z)/U_{mf}$ at the bed center calculated using Eq. (10) with experimental data is shown in Fig. 13. The standard deviation of the fitted values of $(L_{ef}/\tau_{zc})/U_{mf}$ with this equation was only 3.3 %.

The value of $(L_{ef}/\tau_{zw})/U_{mf}$ could be calculated using the following equation:

$$(L_{ef}/\tau_{zw})/U_{mf} = (L_{ef}/\tau_{zwo})/U_{mf} - 0.044(z/h_s)^{0.1} \times (U_s/U_{mf})^{0.3}\{\exp[0.2(z/h_s)]\}(H/1000)^{1.2}, \qquad (11)$$

where $(L_{ef}/\tau_{zwo})/U_{mf} = 0.284(z/h_s)^{0.2}(U_s/U_{mf})^{0.5} \times \exp[0.12(U_s/U_{mf})]$ is the $(L_{ef}/\tau_z)/U_{mf}$ value at the bed wall without an applied magnetic field. A comparison of $(L_{ef}/\tau_{zw})/U_{mf}$ at the bed wall calculated using Eq. (11) with experimental data is shown

Experimental Data	Results Calculated with Eq. (10)	z/h_s (-)	H (A/m)
+	—	0.312	0
○	—	0.503	0
×	—	0.878	0
△	—	0.312	858
□	—	0.503	858
●	—	0.878	858
▲	—	0.312	1716
■	—	0.503	1716
◇	—	0.878	1716

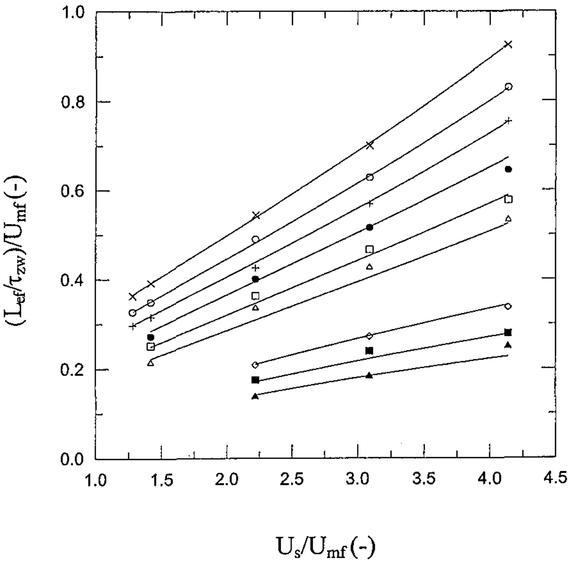

Fig. 13. Comparison of L_{ef}/τ_{zc} calculated with Eq. (10) and experimental data.

Experimental Data	Results Calculated with Eq. (11)	z/h_s (-)	H (A/m)
+	—	0.312	0
○	—	0.503	0
×	—	0.878	0
△	—	0.312	858
□	—	0.503	858
●	—	0.878	858
▲	—	0.312	1716
■	—	0.503	1716
◇	—	0.878	1716

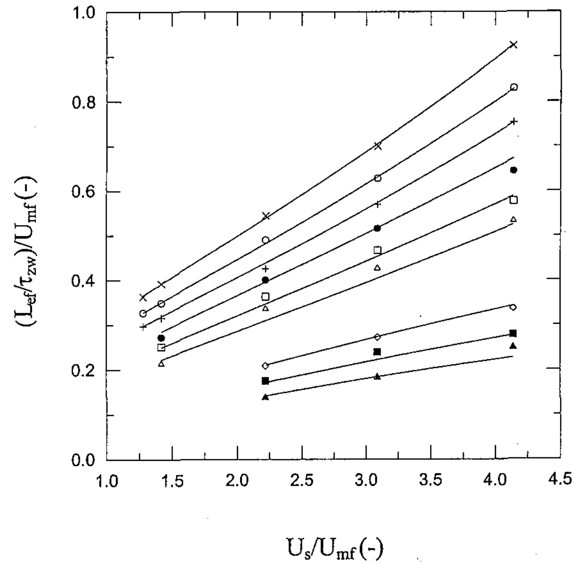

Fig. 14. Comparison of L_{ef}/τ_{zw} calculated with Eq. (11) and experimental data.

in Fig. 14. The standard deviation of the fitted values of $(L_{ef}/\tau_{zw})/U_{mf}$ with this equation was only 3.2%.

The value of B could be calculated using the following equation:

$$B = B_o - 0.22(z/h_s)^{0.1}(U_s/U_{mf})^{0.1} \times \{\exp[-0.04(U_s/U_{mf})]\}(H/1000), \qquad (12)$$

where $B_o = 2.68(z/h_s)^{0.5}(U_s/U_{mf})^{0.5}\exp[-0.4\ (z/h_s) - 0.1\,(U_s/U_{mf})]$ is the B value without an applied magnetic field. A comparison of the B values calculated using Eq. (12) with those calculated using Eq. (8) is shown in Fig. 15. The standard deviation of the fitted values of B with this equation was only 2.0%.

The $(L_{ef}/\tau_z)/U_{mf}$ values calculated using Eq. (7) and Eqs. (10)-(12) were qualitatively the same as those obtained by Tsuo and Gidaspow (1990), Tsuji *et al.* (1998) and Lin *et al.* (1985).

A comparison of positive $(L_{ef}/\tau_z)/U_{mf}$ values (moving up particles) calculated using Eq. (8) with the experimental data reported by Lin *et al.* (1985) is shown in Fig. 16. The standard deviation of the fitted values of $(L_{ef}/\tau_z)/U_{mf}$ with this equation was only 8%.

The difference between fixed beds and MSFBs

As Fig. 11(a) shows, the particle velocity in an MSFB was zero and the same as that in a fixed bed. This result is consistent with those in Lee (1991), Katz and Sears (1969), and Rosensweig *et al.* (1981). They reported that fluid turbulence, random solid movements and solid/fluid mixing characterized in conventional fluidized beds but are not present in MSFBs. Though particles in both fixed beds and MSFBs do not move about freely nor do they back-mix, the rheological behaviors of particles in both fixed beds and MSFBs are very different. The drag force of gas acting on particles was found here to be smaller in a fixed bed than in an MSFB because the superficial gas velocity in a fixed bed was smaller than that in an MSFB.

The difference between MSFBs and MBFBs

As shown in Fig. 11(a), the particle velocity in an MSFB was zero due to the lack of bubble movement. The bubble motion was the main source of particle movement in the gas-solid fluidized beds. As shown in Figs. 9-11 except Fig. 11(a), the magnetic

Key	z/h_s (-)	H (A/m)
+	0.312	0
○	0.503	0
×	0.878	0
△	0.312	858
□	0.503	858
●	0.878	858
▲	0.312	1716
■	0.503	1716
◇	0.878	1716

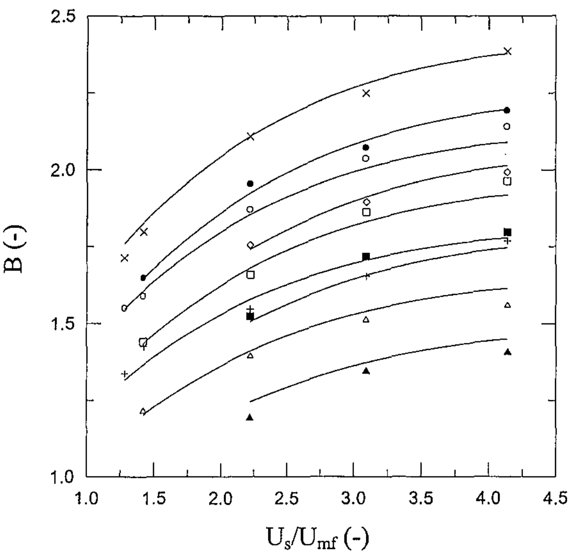

Fig. 15. Comparison of parameter B values calculated with Eq. (12) and with Eq. (8).

field could not suppress bubble formation. The particles in the bed moved freely in the MBFBs due to the bubble motion.

Lee (1983, 1991) defined the so-called jelling point and freezing or solidification point when he characterized the solid-discharge behavior in MSFBs based on an orifice experiment. Lee called the jelling point the point at which the bed becomes sticky. Good solid flowability can be expected below the jelling point. Therefore, the flowability of particles in both MSFBs and MBFBs is almost the same when the magnetic field intensity is below the corresponding jelling point.

The difference between BFBs and MBFBs

As shown in Figs. 7 and 9, the particles in both BFBs and MBFBs moved freely. The particles moved upward in the wake region of bubbles and moved downward in the regions with less bubble activity. However, the bubbles in an MBFB were smaller than those in a BFB (Jovanovic *et al.*, 1989; Jovanovic and Jovanovic, 1993), so the particles in an MBFB obtained less kinetic energy from bubbles than those in a BFB did. At the same superficial gas velocity, the particles in a BFB moved more violently than those in an MBFB did. As shown in Figs.

Experimental Data Reported by Lin *et al.* (1985)	Results Calculated with Eq. (8)	z/h_s
+	—	0.797
○	—	0.929
×	—	1.062
●	—	1.195
✻	—	1.327

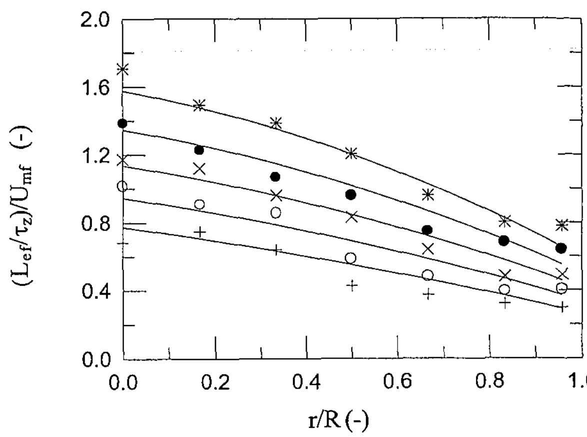

Fig. 16. Comparison of $(L_{ef}/\tau_z)/U_{mf}$ value calculated with Eq. (8) with that reported by Lin *et al.* (1985) (U_s/U_{mf} = 3.31).

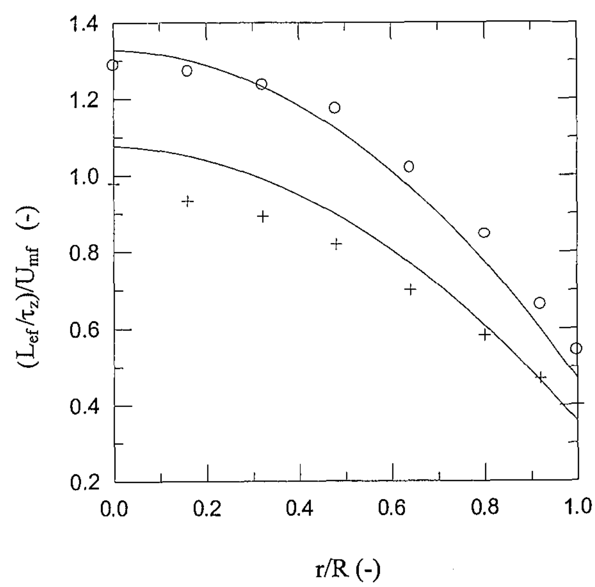

Fig. 17. Computed (—) and experimentally (+, ○) determined $(L_{ef}/\tau_z)/U_{mf}$ (h_s = 0.189 m; z/h_s = 0.878; L = 1m; U_s/U_{mf}= 2.22; (+)H=0 A/m; (○)H= 858 A/m).

9 and 11, in an MBFB at the same superficial gas velocity, the greater magnetic intensity was, the slower was the motion of particles.

Comparison with the results of computer simulation

To make a comparison between the results of this experiment and those obtained with the two-fluid model (continuum model), a simulation of the flow behavior in both a BFB and an MBFB was performed using the Eulerian Granular Multiphase Model with Fluent 4.5 edition software. The finite volume method model was used in this simulation. The details are shown elsewhere (Lin, 2001).

Figure 17 shows the time-averaged particle velocity obtained in the experiments (Figs. 7(b) and 9(b) for rising particles) and simulation results obtained at $U_s / U_{mf} = 2.22$ and $z / h_s = 0.878$. The experimental results were close to those obtained in the computer simulation. The standard deviation at $H = 0$ A/m was 11.6%, and the standard deviation at $H = 858$ A/m was 12.0%. The results of both the experiment and computer simulation showed that the particle velocity in the central bed region was always higher than that near the bed wall, because the particles were carried upwards by rising bubbles and were carried up in their wakes. In addition, the bubbles tended to move toward the bed center.

CONCLUSION

Experimental results for the local particle velocity were obtained in a magnetically fluidized bed for spherical shaped iron particles of Geldart group B powders. The results lead us to draw the following conclusions:

(1) An optical method of analysis has been applied successfully to the study of particle velocity profiles in dense phase.
(2) The local particle velocity in an MFB was dependent on the magnetic field intensity, superficial gas velocity and position in the bed. The particle velocity decreased as the magnetic field intensity and distance from the axis of the bed column increased, and as the superficial gas velocity and distance from the distributor decreased.
(3) In an MBFB (with a 5 cm i.d. and a deeper bed), three flow pattern of particles were observed: (a) the particles circulated as a vortex ring with upflow at the bed axis and down flow at the wall; (b) particles ascended between the bed center and the bed wall, and descended at both the bed center and the bed wall; (c) particles ascended near the bed wall and descended in the bed central region.
(4) A general correlation was developed to predict the axial transit time: $1/\tau_z = 1/\tau_{zc} - (1/\tau_{zc} - 1/\tau_{zw})(r/R)^B$.
(5) The time-averaged particle velocity obtained in the experiment was close to that obtained in the computer simulation. When $U_s / U_{mf} = 2.22$ and $z / h_s = 0.878$, the standard deviation at $H = 0$ A/m was 11.6%, and the standard deviation at $H = 858$ A/m was 12.0%.

NOMENCLATURE

$Ai (i = 1\text{-}6)$	constant
B	parameter in Eq. (8)
B_o	parameter in Eq. (12)
d_b	bubble diameter, m
d_p	mean diameter of particles, m
exp	experimental value
fit	fitted value
H	magnetic field intensity, A/m
H_{ms}	minimum stabilization field (where the curve of the bubble diameter vs. the magnetic field intensity intersects the abscissa, denoted as H_{ms}), A/m
h_s	static bed height, m
L	bed height, m
L_{ef}	effective distance between two light-detecting fibers, m
L_G	geometrical distance between two light-detecting fibers, m
N	total amount of experimental data
R	radius of bed, m
R_{rtt}	distance between the tip of the probe and the center of the rotating bed, m
r	radial coordinate, m
T	period of rotation, s
U_{mf}	minimum fluidization velocity obtained with the graphical method of Davidson and Harrison, m/s
U_s	superficial gas velocity, m/s
V_p	local, time-averaged particle velocity in the bed or the particle velocity in the cylindrical container, m/s
V_t	terminal velocity, m/s
z	height above the distributor plate, m

Greek symbols

θ	flow orientation with respect to the horizontal, rad
τ	transit time, s
τ_r	transit time in the radial direction, s
τ_z	transit time in the axial direction, s
τ_{zc}	transit time in the axial direction at the bed center, s
τ_{zco}	transit time in the axial direction at the bed center without an applied magnetic field, s
τ_{zw}	transit time in the axial direction at the bed wall, s
τ_{zwn}	transit time in the axial direction at the bed wall without an applied magnetic field, s
ω	angular velocity, s^{-1}

Abbreviations

BFB	bubbling fluidized bed

CFB circulating fluidized bed
MBFB magnetized bubbling fluidized bed
MFB magnetofluidized bed
MSFB magnetically stabilized fluidized bed
S.D. standard deviation of the fitted values from the experimental values; see Eq. (9), %

REFERENCES

Botterill, J. S. M. and D. J. Bessant, "The Flow of Fluidized Solids," *Powder Technol.*, **14**, 131 (1976).

Dencs, B., "Particle Velocity Measurements in Dense Fluidized Beds," *Part. Part. Syst. Charact.*, **12**, 314 (1995).

Geldart, D., "Types of Gas Fluidization," *Powder Technol.*, **7**, 285 (1973).

Hamdullahpur, F., M. J. Pegg, and G. D. M. MacKay, "Laser-Fluorescence Technique for Turbulent Two-phase Flow Measurements," *Int. J. Multiphase Flow*, **13**, 379 (1987).

Hartge, E.-U., D. Rensner, and J. Werther, "Solids Concentration and Velocity in Circulating Fluidized Beds," Proc. 2nd Int. Conf. Circulating Fluidized Bed Technology, P. Basu and J. F. Large, Eds., p. 165, Pergamon Press, Oxford, U.K. (1988).

Heertjes, P. M., J. Verloop, and R. Willems, "The Measurement of Local Mass Flow Rates and Particle Velocities in Fluid-Solid Flow," *Powder Technol.*, **4**, 38 (1970/71).

Herbert, P. M., T. A. Gauthier, C. L. Briens, and M. A. Bergougnou, "Application of Fiber Optic Reflection Probesto the Measurement of Local Particle Velocity and Concentration in Gas-Solid Flow," *Powder Technol.*, **80**, 243 (1994).

Horio, M. K., Morishita, O. Tachibana, and N. Murata, "Solid Distribution and Movement in Circulating Fluidized Beds," Proc. 2nd Int. Conf. Circulating Fluidized Bed Technology, P. Basu and J. F. Large, Eds., p. 147, Oxford, U.K. (1988).

Hristov, J. Y., "Fluidization of Ferromagnetic Particles in a Magnetic Field, Part II: Field Effects on Preliminary Gas Fluidized Bed," *Powder Technol.*, **97**, 35 (1998).

Jovanovic, G. N., Z. R. Jovanovic, G. Vunjak-Novakovic, and D. V. Vukovic, "Bubble Size in Magnetically Controlled Fluidized Beds," Fluidization VI, J. R. Grace, L. W. Shemilt and M. A. Bergougmou, Eds., p. 237, Engineerin Foundation, New York, U.S.A. (1989).

Jovanovic, G. N. and Z. R. Jovanovic, "Bubble Size and Fluidization Regimes in Magneticlly Controlled Fluidized Beds," paper no. 28i, paper presented at the 1993 AIChE Annual Meeting, St. Louis, MO, U.S.A. (1993).

Katz, H. and J. T. Sears, "Electric Field Phenomena in Fluidized and Fixed Beds," *Can. J. Chem. Eng.*, **47**, 50 (1969).

Klinzing, G. E., A. Zaltash, and C. A. Myler, "Particle Velocity Measurements through Electrostatic Field Fluctuations Using External Probes," *Part. Sci. Technol.*, **5**, 95 (1987).

Kunii, D. and O. Levenspiel, Fluidization Engineering, Butterworth-Heinemann, Boston, U.S.A. (1991).

Lee, W.-K., "The Rheology of Magnetically Stabilized Solids," *AIChE Symp. Ser.*, **79**(222), 87 (1983).

Lee, W.-K., "A Review of the Rheology of Magnetically Stabilized Beds," *Powder Technol.*, **64**, 69 (1991).

Levy, Y. and F. C. Lockwood, "Laser Doppler Measurements of Flow in Freeboard of a Fluidized Bed," *AIChE J.*, **29**, 889 (1983).

Lin, J. S., M. M. Chen, and B. T. Chao, "A Novel Rodiactive Particle Tracking Facility for Measurement of Solids Motion in Gas Fluidized Beds," *AIChE J.*, **31**, 465 (1985).

Lin, Y. C. "Voidage and Velocity Profiles in Magnetic Fluidized Beds," Ph.D. Thesis, Department of Chemical Engineering, National Taiwan University, Taiwan (2001).

Lin, Y.-C. and L.-P. Leu, "Voidage Profiles in Magnetically Fluidized Beds," *Powder Technol.*, **120**, 199 (2001).

Liu, Y. A., R. K. Hamby, and R. D. Colberg, "Fundamental and Practical Developments of Magnetofluidized Beds: A Review," *Powder Technol.*, **64**, 3 (1991).

Marsheck, R. M. and A. Gomezplata, "Particle Flow Patterns in a Fluidized Bed," *AIChE J.*, **11**, 167 (1965).

Merry, J. M. D. and J. F. Davidson, "Gulf Stream Circulation in Shallow Fluidized Beds," *Trans. Inst. Chem. Eng.*, **52**, 361 (1973).

Morooka, S., K. Kusakabe, N. Ohnishi, F. Gujima, and H. Matsuyama, "Measurement of Local Fines Movement in a Fluidized Bed of Coarse Particles by a Fluorescent Tracer Technique," *Powder Technol.*, **58**, 271 (1989).

Nieuwland, J. J., R. Meijer, J. A. M. Kuipers, and W. P. M. van Swaaij, "Measurements of Solids Concentration and Axial Solids Velocity in Gas-Solid Two Phase Flow," *Powder Technol.*, **87**, 127 (1996).

Oki, K., T. Akehata, and T. Shirai, "A New Method for Evaluating the Size of Moving Particles with a Fiber Optic Probe," *Powder Technol.*, **11**, 51 (1975).

Oki, K., W. P. Walawender, and L. T. Fan, "The Measurement of Local Velocity of Solid Particles," *Powder Technol.*, **18**, 171 (1977).

Patrose, B. and H. S. Caram, "Optical Fiber Transit Anemometer for Particle Velocity Measurements in Fluidized Beds," *AIChE J.*, **28**, 604 (1982).

Rao, V. L. and D. Venkateswarlu, "Determination of Velocities and Flow Pattern of Particles in Mass Flow Hoppers," *Powder Technol.*, **7**, 263 (1973).

Raso, G., G. Tirabasso, and G. Donsi, "Impact Probe for Local Analysis of Gas-Solids Flows," *Powder Technol.*, **34**, 151 (1983).

Rosensweig, R. E., "Fluidization: Hydrodynamic Stabilization with a Magnetic Field," *Science*, **204**, 57 (1979).

Rosensweig, R. E., J. H. Siegell, W.-K. Lee, and T. Mikus, "Magnetically Stabilized Fluidized Solids," *AIChE Symp. Ser.*, **77**(205), 8 (1981).

Stein, M., Y. L. Ding, J. P. K. Seville, and D. J. Parker, "Solids Motion in Bubbling Gas Fluidized Beds," *Chem. Eng. Sci.*, **55**, 5291 (2000).

Tsuji, Y., Y. Morikawa, and H. Shiomi, "LDV Measurements of an Air-Solid Two-Phase Flow in a Vertical Pipe," *J. Fluid Mech.*, **139**, 417 (1984).

Tsuji, Y., T. Tanaka, and S. Yonemura, "Cluster Patterns in Circulating Fluidized Beds Predicted by Numerical Simulation (Discrete Particle Model Versus Two-Fluid Model)," *Powder Technol.*, **95**, 254(1998).

Tsuo, Y. P. and D. Gidaspow; "Computation of Flow Patterns in Circulating Fluidized Beds," *AIChE J.*, **36**, 885 (1990).

Tung, Y., J. Li, and M. Kwauk, "Radial Voidage Profiles in a Fast Fluidized Bed," Fluidization '88, M. Kwauk and D. Kunii, Eds., p. 139, Science Press, Beijing, China (1988).

van Velzen, D. H. J. Flamm, H. Langenkamp, and A. Casile, "Motion of Solids in Spouted Beds," *Can. J. Chem. Eng.*, **52**, 156 (1974).

Werther, J. and O. Molerus, "The Local Structure of Gas Fluidized Beds-II: The Spatial Distribution of Bubbles," *Int. J. Multiphase Flow*, **1**, 123 (1973).

Xia, Y.-S., H.-Z. Li, and C.-G. Zheng, "Extreme Value Estimation of Cluster Size in a Fast Fluidized Bed," *Eng. Chem. Metal.* (China) (in Chinese), **14**(3), 245 (1993).

Yang, Y. L., Y. Jin, Z. Q. Yu, and Z. W. Wang, "Investigation on Slip Velocity Distribution in the Riser of Dilute Circulating Fluidized Bed," *Powder Technol.*, **73**, 67 (1992).

Yianneskis, M., "Velocity, Particles Sizing and Concentration Measurement Technique for Multi-Phase Flow," *Powder Technol.*, **49**, 261 (1987).

Zhang, W., Y. Tung, and F. Johnsson, "Radial Voidage Profiles in Fast Fluidized Beds of Different Diameters," *Chem. Eng. Sci.*, **46**, 3045 (1991).

Zhang, H. and J. X. Zhu, "Hydrodynamics in Downflow Fluidized Beds (2): Particle Velocity and Solids Flux Profiles," *Chem. Eng. Sci.*, **55**, 4367 (2000).

(Manuscript received Apr. 7, 2005, and accepted Jul. 13, 2005)

磁流體化床中粒子之速度與運動情況

林永忠　呂理平
國立台灣大學化學工程學系

摘　要

本研究利用 230 μm 之鐵粒子探討在磁流體化床中之粒子速度與粒子在床中之運動情況。磁流体化床中之均匀磁場利用直流電通過五個線圈產生。光纖探針被設計用來量測鐵粒子在磁流體化床中不同之位置，不同氣體表面速度與不同之磁場強度下之速度。

實驗結果顯示在磁穩流體化床(MSFB)中之粒子速度爲零。在磁氣泡流體化床(MBFB)中粒子速度隨磁場強度之增加而減少；隨床中徑向距離之增加而減少；隨床中氣體表面速度之減少而減少；以及隨床中距離分配板之距離增加而增加。粒子之速度與方向可以利用以下公式計算：$V_p = L_{ef} /(\tau_r^2 + \tau_z^2)^{1/2}$ ，$\theta = \tan^{-1}(\tau_z / \tau_r)$ 。而軸向經過時間 τ_z 可以下式表示：$1/\tau_z = 1/\tau_{zc} - (1/\tau_{zc} - 1/\tau_{zw})(r/R)^B$ 。其中 τ_{zc} , τ_{zw} , B 皆與床中氣體表面速度磁場強度以及隨床中距離分配板之距離有關，並且皆可以用下式表示 $A1(z/h_s)^{A2}(U_s/U_{mf})^{A3}\{\exp[A4\ (z/h_s) + A5\ (U_s/U_{mf})]\}H^{A6}$ 實驗結果與模擬計算結果非常相近。